ORNL/TM-2022/2779

Estimation of High-Altitude Electromagnetic Pulse Signal Leakage into Power Generation Facilities: Simulations and Measurements

DaHan Liao
Zhi Li
Yilu Liu
Lawrence C. Markel
Benjamin W. McConnell
Brian R. Poole
Lisa Wang

December 2022

OAK RIDGE National Laboratory

ORNL IS MANAGED BY UT-BATTELLE LLC FOR THE US DEPARTMENT OF ENERGY

ORNL/TM-2022/2779

Energy Science and Technology Directorate
Electrification and Energy Infrastructures Division

ESTIMATION OF HIGH-ALTITUDE ELECTROMAGNETIC PULSE SIGNAL LEAKAGE INTO POWER GENERATION FACILITIES: SIMULATIONS AND MEASUREMENTS

DaHan Liao
Zhi Li
Yilu Liu
Lawrence C. Markel
Benjamin W. McConnell
Brian R. Poole
Lisa Wang

December 2022

Prepared by
OAK RIDGE NATIONAL LABORATORY
Oak Ridge, TN 37831
managed by
UT-Battelle LLC
for the
US DEPARTMENT OF ENERGY
under contract DE-AC05-00OR22725

CONTENTS

LIST OF FIGURES

LIST OF TABLES

ABBREVIATIONS

CW	continuous wave
HEMP	high-altitude electromagnetic pulse
ORNL	Oak Ridge National Laboratory
PEC	perfect electrical conductor
RF	radio frequency
UHF	ultra high frequency
VHF	very high frequency

ABSTRACT

The coupling of early-time high-altitude electromagnetic pulse signals into a power generation facility was investigated. This study encompasses both electromagnetic simulation and on-site experimental efforts that are relevant to shielding effectiveness estimation with a passive technique. As an initial step in understanding the attenuation models involved, simulations were carried out as a function of frequency, building properties, and signal incidence angle. Testing was then performed at the US Department of Energy's Oak Ridge National Laboratory campus to identify the equipment needed for signal collection and to fine-tune the experimental procedure. Finally, as an application of the models and methods presented, measurements were conducted at a power generation plant to derive the field transfer functions and coupled high-altitude electromagnetic pulse waveforms for various locations within the facility.

1. INTRODUCTION

A systematic approach is needed to evaluate high-altitude electromagnetic pulse (HEMP) signal leakage into power generation plants. The traditional method of determining facility shielding effectiveness is to use a radiated continuous wave (CW) test (i.e., an active test) [1] in which a comparison is made between internal and external signal levels to deduce the building attenuation across different frequencies. Although such a test is the preferred technique for estimating the electromagnetic coupling transfer function (both its magnitude and its phase) of a building, it may not be convenient to implement. The potential barriers to practicality include (1) the need to acquire regulatory permission to transmit high-power signals, often over a wide frequency band; (2) the concern that the transmitted signals required for testing may interfere with existing communications and control systems within the facility; (3) the requirement to place the transmitting antenna in the far field zone to establish plane wave illumination; and (4) the realization that, at the lower frequency range, the transmitting antenna would have to be very large, or else it would have very low efficiency/gain; for instance, the top-loaded monopole antenna used by Sandia National Laboratories for an active test performed at a nuclear plant had dimensions $30 \times 7.3 \times 1.8$ m [2]. Therefore, in view of the described issues, a high-fidelity, comprehensive radiated test is not easy to set up in practice, and the facility itself may impose certain constraints (e.g., limitations related to physical location, operation conditions) that would prevent such a test from being carried out at all.

Shielding effectiveness testing has been addressed in the military standards for protecting ground-based facilities against HEMP signals. In particular, two configurations of the active approach for estimating signal penetration are considered in MIL-STD-188-125-1 Appendices A and C [3]. The setup in Appendix A (Figure 1) is more suitable for determining leakage through a simple electromagnetic barrier than for applications that involve a HEMP signal, since the latter assumes a plane wave mode of illumination. In Appendix C, the elements of a CW immersion test (Figure 2) are put forth in detail. To emulate a HEMP signal in this case, the distance between the transmitter and the building, R, must satisfy the following relationship to ensure far field plane wave excitation:

$$R > max\left(\lambda_{max}, \frac{2D^2}{\lambda_{min}}\right) \tag{1}$$

where λ_{min} and λ_{max} are the minimum and maximum wavelengths, respectively, and D is the maximum dimension of the building. For typical scenarios, the separation needed between the transmitter and the building is on the order of kilometers. As a conservative example, for a frequency range of 1–50 MHz, for a facility such as the powerhouse considered in Section 4., with dimensions $\sim 122 \times 52 \times 52$ m, it can be shown that $R > 6.8$ km. Evidently, this distance requirement is rather prohibitive.

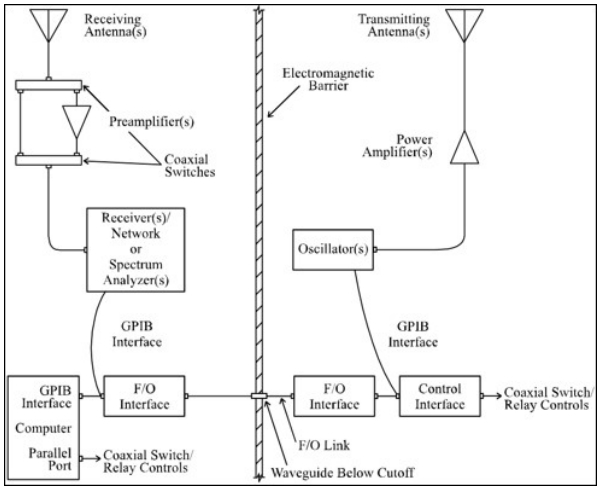

Figure 1. MIL-STD-188-125-1 Appendix A.

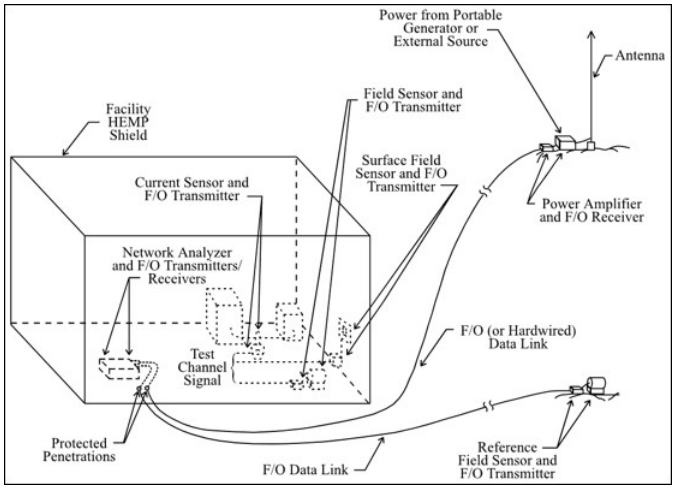

Figure 2. MIL-STD-188-125-1 Appendix C.

Given the aforementioned drawbacks of the active test, an alternative method for deducing shielding effectiveness has been advocated by [4; 5; 6]. The proposed test (i.e., a passive test) is established by using existing radio frequency (RF) sources of opportunity (e.g., broadcast radio/TV, cellular) in the ambient environment as illuminators (Figure 3). Although such a test is simpler and less expensive to set up than the CW active test, it does have the following disadvantages: (1) the number of frequency points available may be limited; (2) the illumination angle and polarization state cannot be controlled; and (3) the results are expected to be less accurate than those from an active test. Despite these shortcomings, a passive test as described would still be useful, especially when augmented with modeling and simulation data, for deriving a first order estimate of HEMP coupling into a facility. Of course, if no suitable ambient RF sources can be found at the test site, or if the sources present are not sufficiently strong or stable, then conducting the passive test would not be possible.

Notably, the technique for evaluating signal penetration employed in this work is similar to those others have implemented over the years for non-HEMP applications such as radio/cellular communications

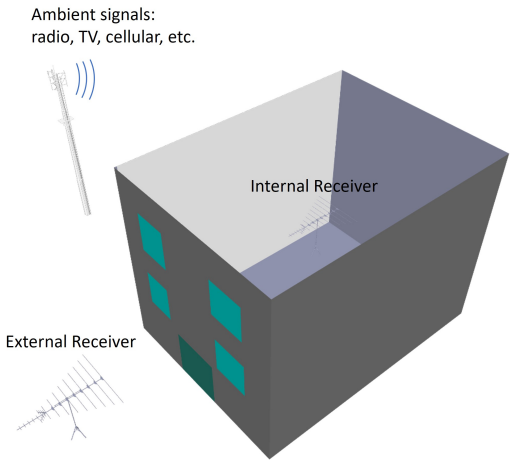

Figure 3. Passive test for assessing signal penetration.

coverage and electromagnetic compatibility. Examples of empirical investigations that have considered the attenuation of external electromagnetic fields by structures such as residential housing and commercial buildings can be found elsewhere [7; 8; 9; 10; 11; 12]. However, most of these works focus on frequencies that are higher than those relevant for HEMP.

The objective of this study was to apply the passive test to determine the characteristics of the HEMP component leaked into a power generation facility. The following discussion summarizes the equipment required for such a test and the general procedure to be followed.

1.1 EQUIPMENT FOR A PASSIVE TEST

The equipment includes antennas (with sufficient gain, but reasonably sized to be moved around easily), antenna stands, portable spectrum analyzers (preferably ones that can be powered by a laptop via the USB port), a laptop, and a utility cart. For a more sensitive setup, for receiving signals below 30 MHz, a magnetic ferrite or electric monopole antenna (or both) should be used. To expedite a measurement campaign consisting of many sampling positions both inside and outside of the facility, spectrum analyzer control and data collection should be automated as much as possible, such as by using a MATLAB script, so that the operator only has to move the utility cart carrying the instrumentation to a location, run the script to collect/save the data, and then move to the next location.

1.2 GENERAL PROCEDURE OF A PASSIVE TEST

Once a power generation plant has been identified, before any actual test, the types of signal sources that are expected to be present at the plant location should be assessed. Because broadcast radio/TV and cellular radiators are required to register with the Federal Communications Commission, emitter information, including the exact location of the transmitter antenna/radio tower and the transmitted power levels, is usually publicly available online. Simple propagation studies can also be performed to evaluate whether a particular transmitter can provide sufficient incident power at the testing site to allow meaningful attenuation calculations to be made. This pre-test survey could also serve as a screener to determine whether a particular plant is a good candidate for the passive test.

Actual testing at the facility would entail RF spectrum sampling at both external and internal facility locations. For the external sampling, measurements should be taken around the perimeter of the facility (e.g., at four sides of a building). Internal sampling can be conducted at all indoor locations of interest (e.g., control rooms). All the measurement paths should be determined a priori based on a layout of the plant. To capture the signal constructive and destructive interference patterns (and multipath effects), many sampling locations may be needed. For the current application, although there is no proven rule-of-thumb formulation that can be used to readily determine a suitable spatial sampling interval, a sampling interval of approximately 2 to 3 m provides a reasonable balance between data collection expediency and fidelity. Of course, if time and resources permit, finer sampling can always be applied and would lend additional confidence to the data. In general, because most settings are multipath-rich environments, the actual signal level can vary significantly (e.g., by >10 dB) from one location to the next—even with a separation distance of a few feet—and can fluctuate a few decibels from one spectrum sweep to the next for a fixed location. In terms of the frequency range, for this study, ambient signals primarily in the band of ~1 to 200 MHz were examined. Although the main interest here concerns the early-time HEMP signal, propagation at the higher frequencies was also tangentially considered since those frequencies would be relevant for intentional electromagnetic interference waveforms, such as those emitted from high-power microwave transmitters [13; 14].

From the data collected, a shielding effectiveness can be defined in terms of the average received powers as

$$S\,[\mathrm{dB}] = P_{external}[\mathrm{dB}] - P_{internal}[\mathrm{dB}] \tag{2}$$

which can be formulated for the electric or magnetic field. Examples of "typical" transfer functions are shown in Figure 4 for a closed enclosure, which demonstrates that, in general, the overall response can be loosely partitioned into three domains: a low-frequency region, a resonance region, and a high-frequency region. In the low-frequency region, for frequencies below the ~10–20 MHz range, the coupling coefficient is an algebraic function of the frequency with an asymptotic form of $\propto f^n$ ($n = 0, 1, 2, \ldots$). In this regime, the electric field attenuation is greater than the magnetic field attenuation, and the difference increases with decreasing frequency [7]. In the resonance region, the electric and magnetic field attenuation levels can likely be simply taken to be almost the same (in the average sense). In the high-frequency region, the field intensity exponentially decays as a function of frequency.

Although it would be beneficial to measure the signal response as a function of the antenna orientation (i.e., both horizontal and vertical), there is likely no significant difference in the average attenuation between the different orientations when the data from multiple locations are averaged together, especially for indoor locations, where the fields are more randomly polarized.

Carrying out the internal and external signal sampling at around the same time is preferred because some transmitters may vary their transmitted power during the day. For example, cellular transmitters tend to transmit higher powers when the user traffic is high [15]. Most AM radio stations are also required by the Federal Communications Commission to reduce their power at night.

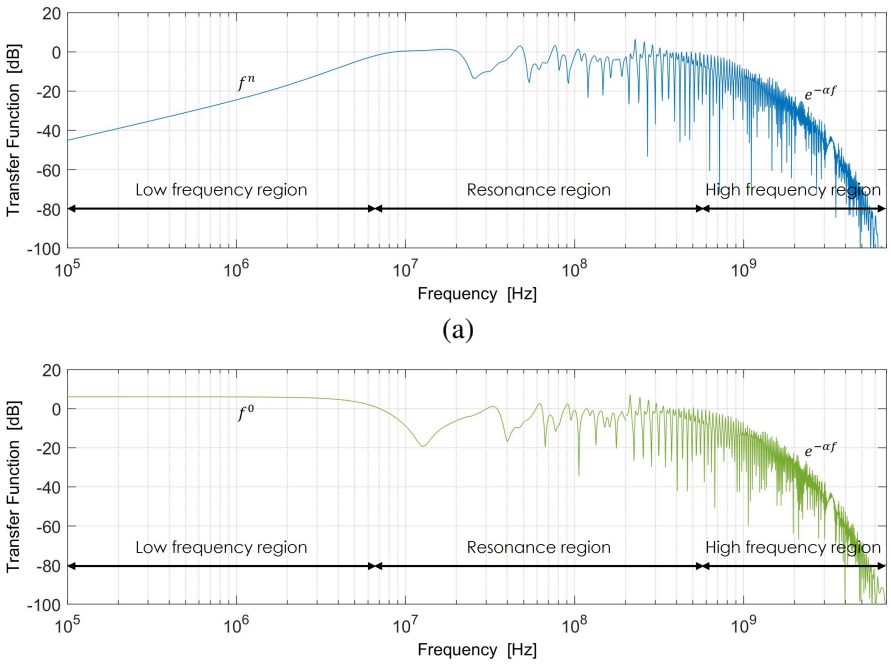

Figure 4. Examples of "typical" transfer functions for a closed enclosure: (a) electric; (b) magnetic.

2. ELECTROMAGNETIC SIMULATIONS

To gain an initial insight into the propagation characteristics of facilities, 3D numerical simulations of canonical building structures were carried out. An integral equation-based code (i.e., the method of moments [16]) as implemented by a commercial software [17] was applied to understand the interactions of electromagnetic waves with structures as a function of frequency, excitation incidence angle, building/ground plane electrical properties, and building dimensions. Because the simulations rely on a full-wave approach, there are no restrictions on the types of construction material that can be incorporated into the model. However, the electrical size of the overall computational domain may be limited by the computational resources available. An example simulation setup and its results are shown in Figure 5.

2.1 MODEL SETUP

In all the following simulations, the external excitation was provided by a plane wave with incidence angle θ_i. A vertically polarized incoming wave was assumed since, in practice, vertically polarized signals generally experience less propagation loss in an outdoor environment. The electric and magnetic fields were first recorded at observation points located inside and around the building structure; then, the shielding effectiveness levels (or transfer functions) were derived from Eq. (2) using the field responses. The maximum frequency was set to 20 MHz because of computational resource constraints, which is an acceptable limit given that most of the energy of the standard early-time HEMP is in the low-frequency region.

The simulation models considered in detail are shown in Figure 6. The base material of the building walls

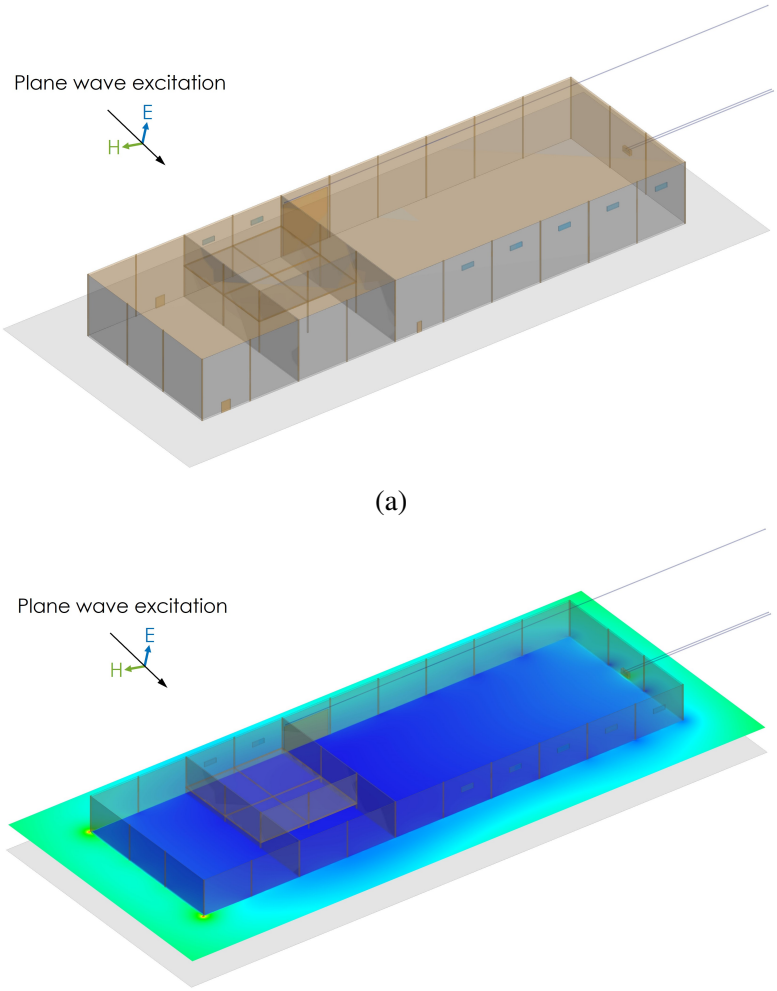

Figure 5. Full-wave simulation example for a building: (a) model; (b) internal and external field intensity plot.

is concrete with relative dielectric constant $\epsilon_r = 4.5$ and conductivity $\sigma = 20$ mS/m. The wall thickness is 20 cm. The top and the floor of the structure are also concrete, except for the model in Figure 6(b), which assumes a metal roof, along with a wall frame that consists of vertical metallic strips. 2D strips were employed since fully 3D columns and trusses would incur additional computational cost; at the frequency range of interest, this is a reasonable approximation. The exterior ground plane is either a perfect electrical conductor (PEC) or a dielectric surface with $\epsilon_r = 10$ and $\sigma = 1$ mS/m. Models with a dielectric ground plane require finer discretization and more computational resources, especially for convergence at low frequencies. The spatial field sampling interval along interior and exterior paths is ~2 m, which is comparable to that for the measurement data presented in Section 3..

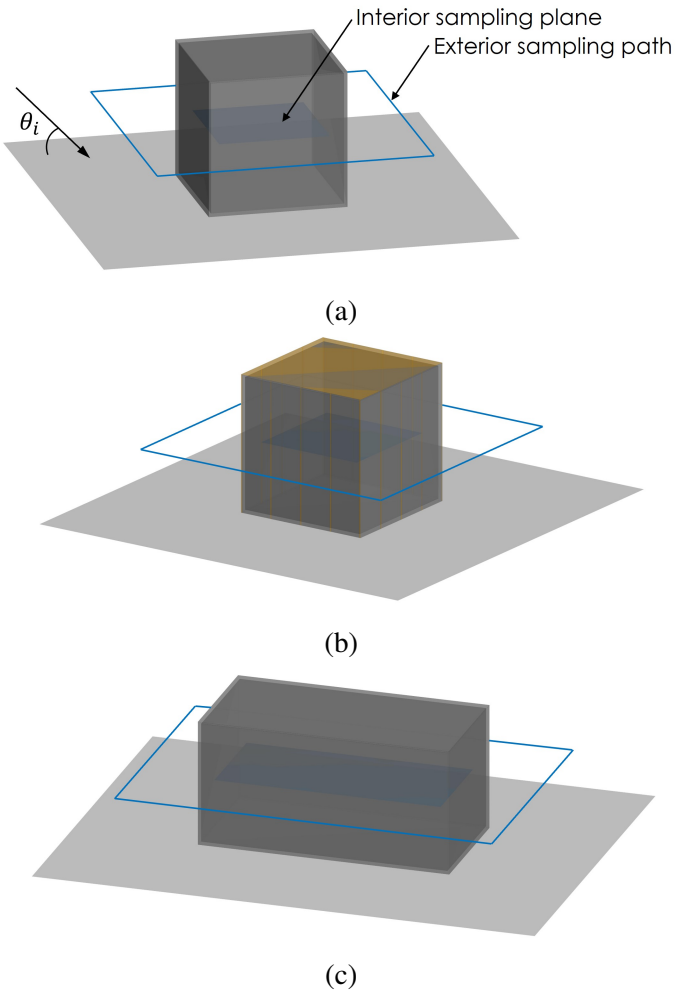

Figure 6. Canonical structures considered in the simulations: (a) 10 × 10 × 10 m (all concrete); (b) 10 × 10 × 10 m (concrete with metal roof/frame); (c) 20 x 10 x 10 m (all concrete).

2.2 SIMULATION RESULTS

The simulation results for the three models in Figure 6 are shown in Figures 7–9. By noting the general trends in the shielding behavior, suitable functions can be constructed in fitting the measurement data—a necessary step in generating a continuous response to evaluate the fields coupled into the interior of a facility. Thus, the following observations can be gleaned from the data. The magnetic transfer function tends to behave as $\propto f^0$ at low frequencies, mostly independent of the excitation incidence angle and the ground plane properties; on the other hand, the electric transfer function is of the form $\propto f^n$ $(n = 0, 1, 2, ...)$ at low frequencies, depending on the incidence angle and ground plane properties. The ground plane (that is, either PEC or dielectric) does not affect the field response significantly for incidence angles away from normal; notably, the ground plane properties seem to affect the results for a building with metal frame more than the other cases. The effects of the ground plane are more evident for the electric response at normal incidence angle ($\theta_i = 90°$), which is partially because for a PEC ground plane, the electric field component

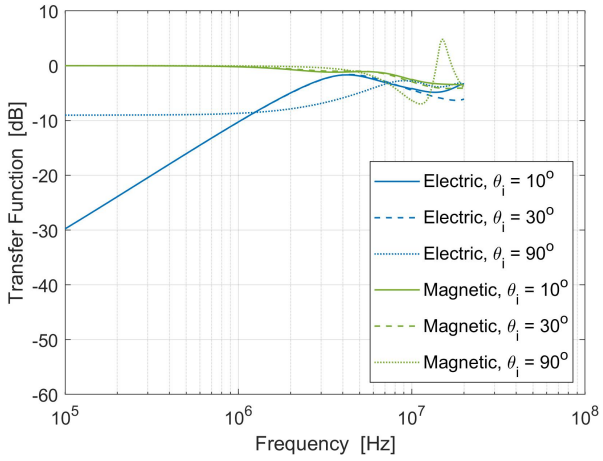

(a)

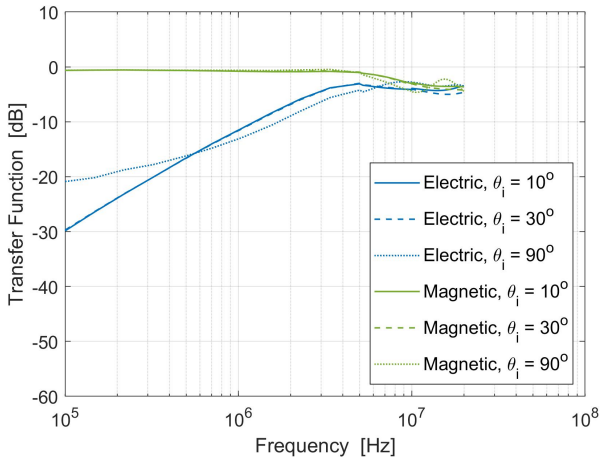

(b)

Figure 7. Transfer functions for the structure in Figure 6(a): (a) PEC ground plane; (b) dielectric ground plane.

that is parallel to the ground—the dominant field component at normal incidence—approaches zero at the same rate for both interior and exterior locations. Therefore, the ratio of the two also approaches a constant as the frequency decreases. The PEC and dielectric ground plane results tend to diverge more (in most cases) as the frequency approaches the resonance region. Furthermore, the metal roof/frame increases shielding against the electric field more than the magnetic field. In addition, the size of the building does not seem to significantly affect the results (for the two sizes considered), except for the electric response of a configuration with a metallic ground plane and at normal incidence.

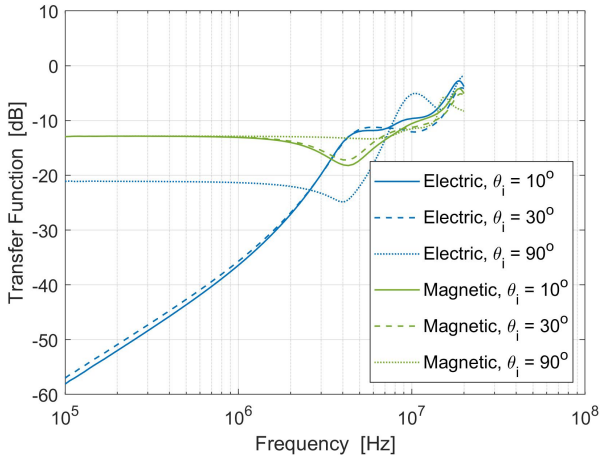

(a)

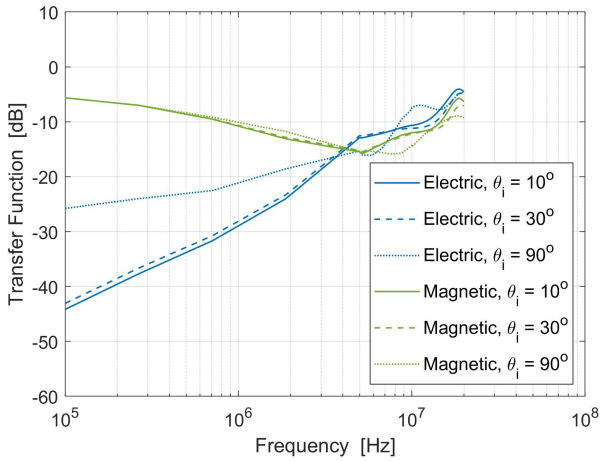

(b)

Figure 8. Transfer functions for the structure in Figure 6(b): (a) PEC ground plane; (b) dielectric ground plane.

3. EXPERIMENTS ON ORNL CAMPUS

As a test run of the passive technique for estimating signal leakage into a building, spectrum sensing was carried out at the ORNL campus, in and around Building 2370HVC (Figure 10(a)). For shielding effectiveness determination, three sets of measurements were taken: (1) a high-band, electric field measurement with an ETS mini-bicon; (2) a low-band, electric field measurement with a retractable monopole (vertically oriented); and (3) a low-band, magnetic field measurements with an AHS ferrite rod (HFR-2). It was assumed that the electric and magnetic field responses start to converge in the resonance region (that is, they have approximately the same level of shielding); therefore, there was no need to conduct a separate measurement for the magnetic field at the high frequency bands. In the low-frequency region, the two field responses diverge and thus were measured separately.

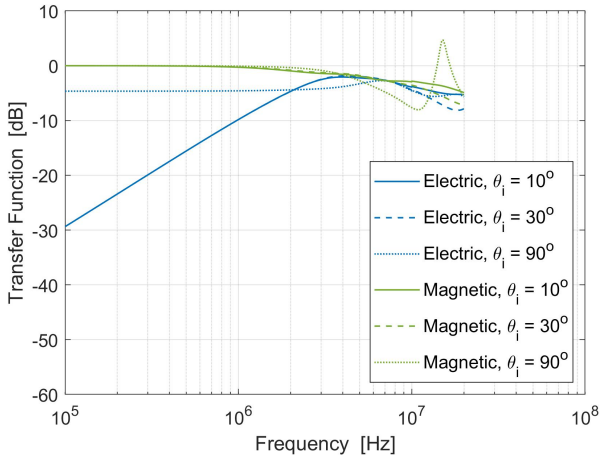

(a)

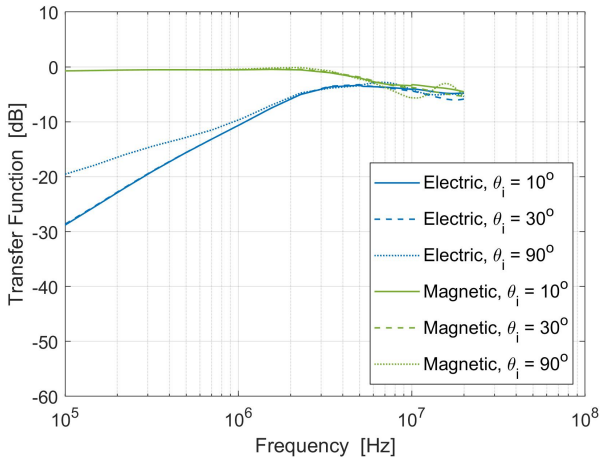

(b)

Figure 9. Transfer functions for the structure in Figure 6(c): (a) PEC ground plane; (b) dielectric ground plane.

An amplifier was not used in the receiver chain during this test, except for the observations taken with the AHS ferrite rod. In all cases, the signal from the antennas was routed to either a Tektronix RSA 306B spectrum analyzer or a Red Pitaya STEMLab 125-14 software-defined radio unit. To automate the data collection process, a MATLAB script—which employed the capabilities of the Instrument Control Toolbox—was applied to control the receiver units.

Figure 11 shows the antennas and the equipment used for the experiments. Measurements were made along two paths—one inside the building and one around the exterior perimeter of the building, as shown in Figure 10(b). The average spatial separation between successive samples was approximately 2 m. For the ferrite rod measurements, at each location, data for four different horizontal orientations were collected and saved, but only the strongest of the four signals was used in the shielding effectiveness calculations.

(a)

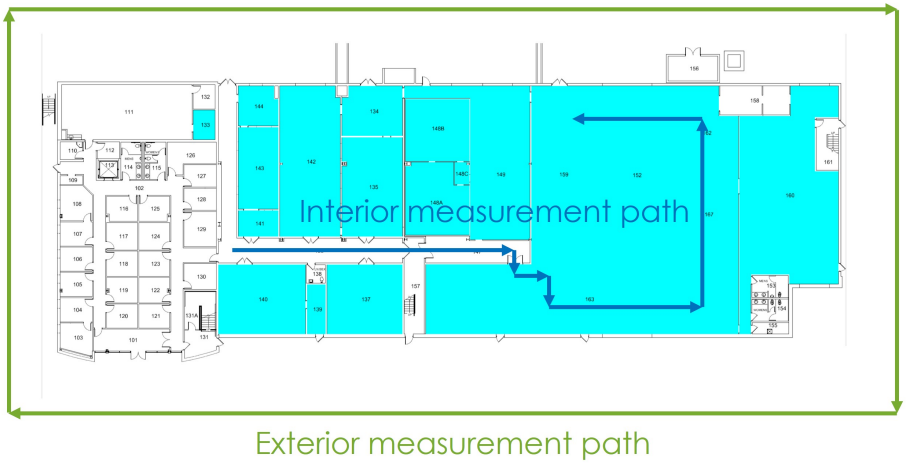

(b)

Figure 10. Building 2370HVC and measurement paths.

3.1 MEASUREMENT DATA FOR AMBIENT ENVIRONMENT

The measurement results are shown in Figures 12–15 as a function of location and frequency. The high-band, electric field data are displayed in Figure 12 for 10–200 MHz, which is a band that contains broadcast FM radio and very high frequency (VHF) TV signals, and in Figure 13, which captures the response at the cellular (GSM downlink) band of 850–900 MHz. The low-band, electric and magnetic field data, which include only the AM radio signals, are shown in Figures 14 and 15, respectively. RF interference signals were encountered, especially for some building interior locations, for all three measurement sets; however, these spurious signals, for the experimental setup as described, did not seem to significantly affect the dynamic range of the data collection.

By averaging the interior and exterior fields at all locations, the shielding effectiveness of the building can be determined as a function of frequency, as displayed in Table 1. The results are consistent with the

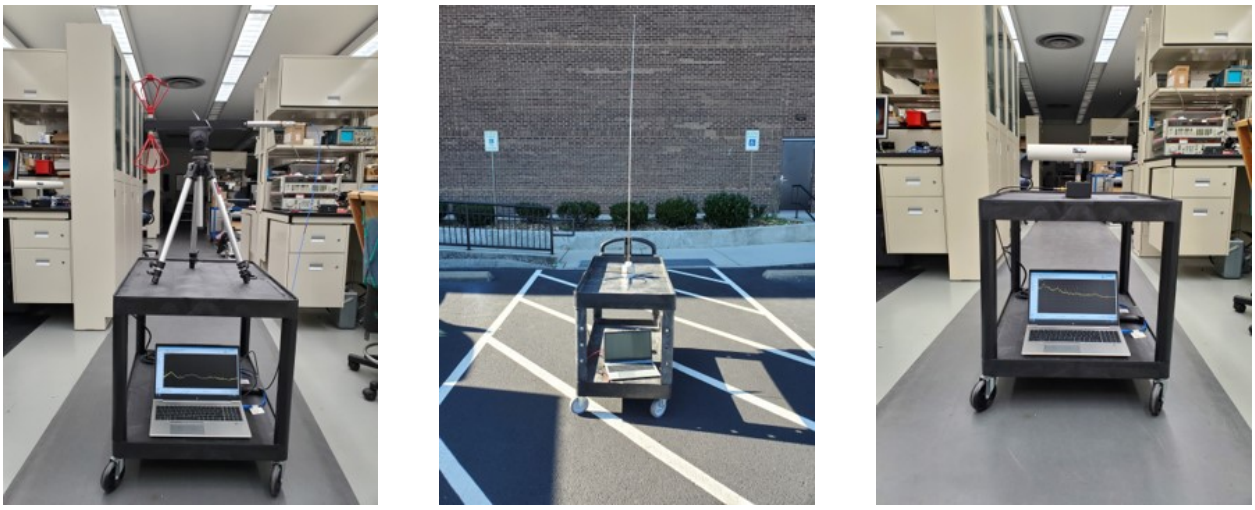

(a) **(b)** **(c)**

Figure 11. Antennas and equipment: (a) ETS mini-bicon; (b) retractable monopole; (c) AHS ferrite rod.

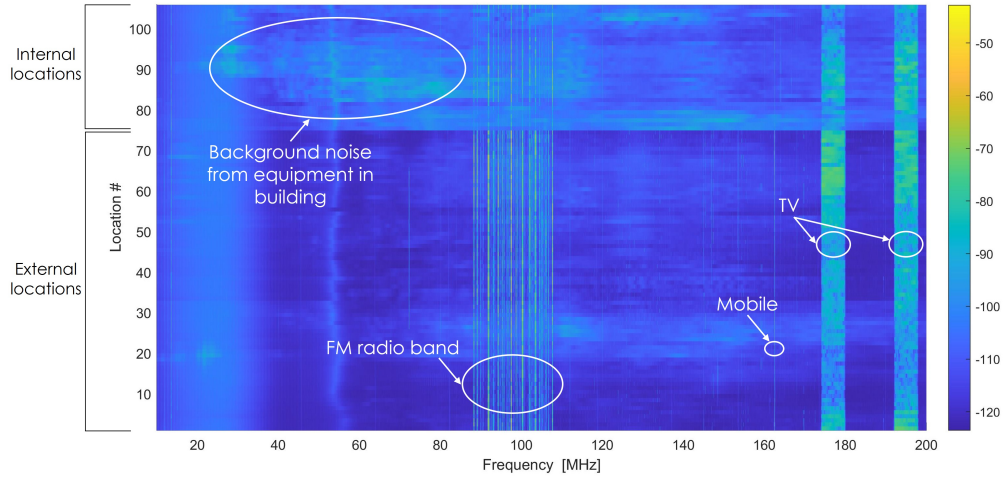

Figure 12. High-band, electric field response for Building 2370HVC.

typical transfer functions in Figure 4.

In view of the simulation results presented in Section 2., the shielding effectiveness results were fitted with standard functions; specifically, the following expressions were applied for the electric and magnetic responses, respectively [6]:

$$S_E(f) = S_{E,\infty}\left(1 + \left(\frac{f_{E,0}}{f}\right)^2\right) \tag{3}$$

$$S_H(f) = S_{H,0}\left(\frac{\left[1 + \left(\frac{f}{f_{H,0}}\right)^2\right]}{\left[1 + \left(\frac{f}{f_{H,1}}\right)^2\right]}\right) \tag{4}$$

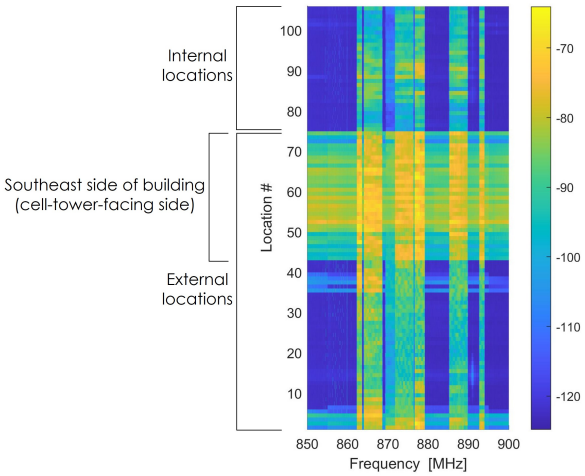

Figure 13. High-band, electric field response for cellular (GSM downlink) band for Building 2370HVC.

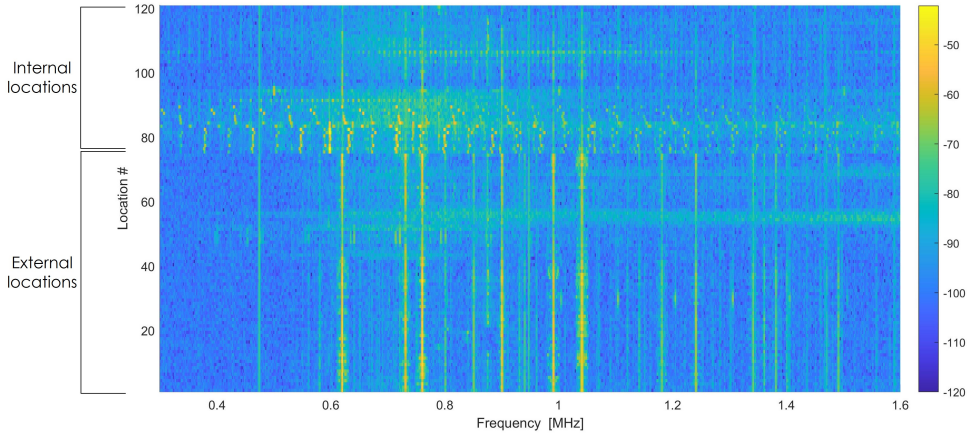

Figure 14. Low-band, electric field response for Building 2370HVC.

where $S_{E,\infty}$ is the electric shielding limit at high frequencies and $S_{H,0}$ is the magnetic shielding limit at low frequencies; $f_{E,0}$, $f_{H,0}$, and $f_{H,1}$ are the 3 dB frequency "knee" points that denote the demarcation between the different spectral regions. Subsequently, the transfer functions can be defined as

$$T_{E,H}(f)\ [\text{dB}] = -10\log_{10} S_{E,H}(f) \tag{5}$$

An example plot of the electric and magnetic transfer functions is shown in Figure 17. Circuit equivalents can also be synthesized to provide a physical interpretation of the shielding functions. It can be shown that Eq. (3) is related to the transfer function for a one-capacitor, two-resistor model, whereas Eq. (4) can be derived from a one-capacitor, three-resistor model.

Figure 16 shows the fitted transfer functions alongside the original measurement data taken at Building 2370HVC. The parameters of the shielding functions are $S_{E,\infty} = 2.28$, $f_{E,0} = 6.61$ MHz, $S_{H,0} = 7.02$, $f_{H,0} = 3.33$ MHz, and $f_{H,1} = 1.9$ MHz.

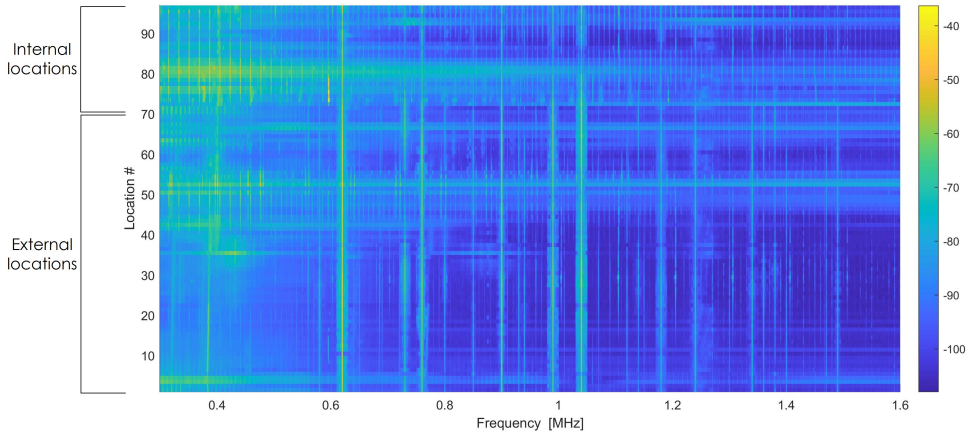

Figure 15. Low-band, magnetic field response for Building 2370HVC.

Table 1. Shielding effectiveness (in decibels) for Building 2370HVC

AM Radio (~1 MHz)	FM Radio (~100 MHz)	VHF TV (~200 MHz)	Cellular (~900 MHz)
15 (7)	11	1	18

Electric ┘ └ Magnetic

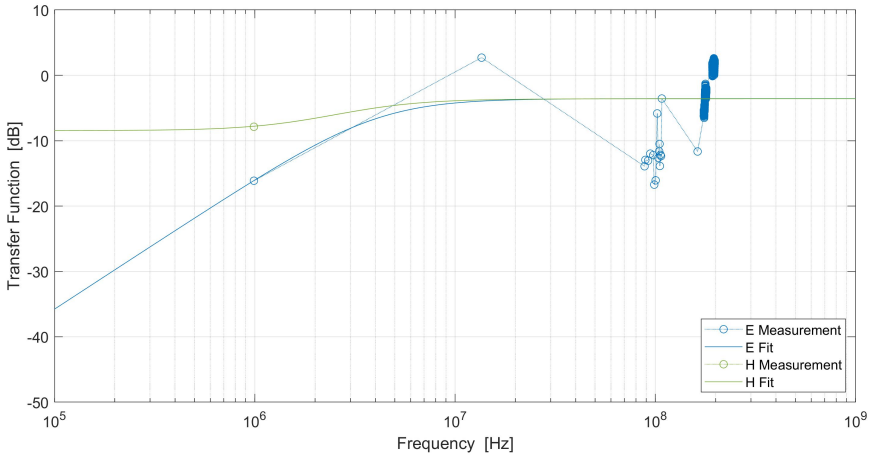

Figure 16. Transfer functions for Building 2370HVC.

3.2 CALCULATION OF BUILDING INTERIOR FIELDS USING SEMI-EMPIRICAL TRANSFER FUNCTIONS

Once the transfer functions are known, the fields inside the building can be derived for any external excitation. Here it was assumed that the excitation is provided by a plane wave that emulates the standard IEC E1 HEMP waveform [18; 19], with the electric field given by

$$E_1(t) = E_{01} k_1 \left(e^{-b_1 t} - e^{-a_1 t} \right) \tag{6}$$

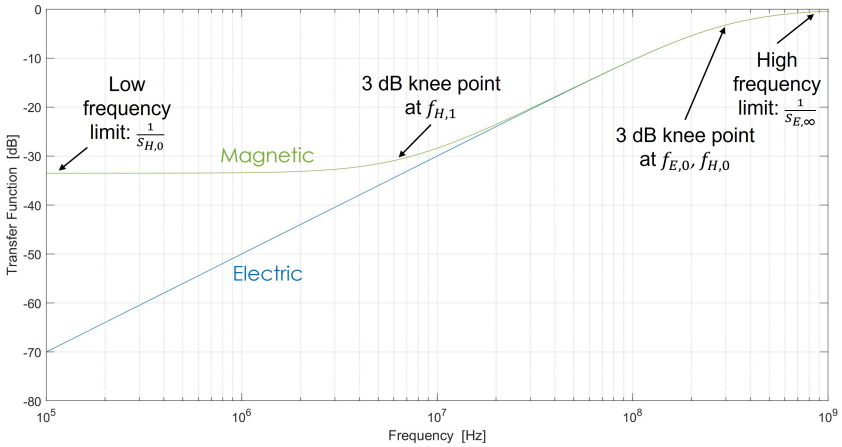

Figure 17. Standard transfer functions.

Table 2. Characteristics of the E1 HEMP waveform

Waveform peak	$E_{peak} = 50000$ V/m
Spectrum peak	$E_{low\ freq} = 0.00152$ V/m/Hz
Waveform peak power	$P_{peak} = 6.64 \times 10^6$ W/m^2
Spectrum peak power	$P_{low\ freq} = 6.11 \times 10^{-9}$ W/m^2/Hz
Total energy	$W_{total} = 0.115$ J/m^2
Time of peak	$t_{peak} = 4.84$ ns
Rise time (10% to 90% of peak)	$t_r = 2.47$ ns
Pulse width (full width at half maximum)	$t_w = 23$ ns
Pulse width (total energy over peak power)	$W_{total}/P_{peak} = 17.3$ ns
Spectrum width (total energy over peak spectrum power)	$W_{total}/P_{low\ freq} = 18.8$ MHz

where $E_{01} = 50$ kV/m, $k_1 = 1.3$, $a_1 = 6 \times 10^8$ s, and $b_1 = 4 \times 10^7$ s; in the frequency domain, this is represented as

$$E_1(f) = E_{01} k_1 \frac{a_1 - b_1}{(a_1 + j2\pi f)(b_1 + j2\pi f)} \tag{7}$$

The corresponding magnetic field waveform was found by normalizing Eqs. (6) and (7) by the free-space impedance. The E1 pulse function in time and frequency domains is shown in Figure 18, and the main characteristics are summarized in Table 2.

Consequently, the total field response in the building can be calculated as

$$E_{total}(f) = E_1(f) \cdot T_E(f) \cdot W_{hs,E}(f) \tag{8}$$

$$H_{total}(f) = H_1(f) \cdot T_H(f) \cdot W_{hs,H}(f) \tag{9}$$

where $W_{hs,E}(f)$ and $W_{hs,H}(f)$ are the half-space responses (that is, the responses at the observation point in the presence of only earth/ground), which can be formulated in closed-form for plane-wave excitation [20]. The time-domain equivalents of Eqs. (8) and (9) can be recovered with the fast Fourier transform algorithm.

Only the amplitude component of $T_E(f)$ and $T_H(f)$ (as computed from $S_E(f)$ and $S_H(f)$) is measured, and a phase term is needed to get a physical (causal) response: here, the phase term was assumed to be that

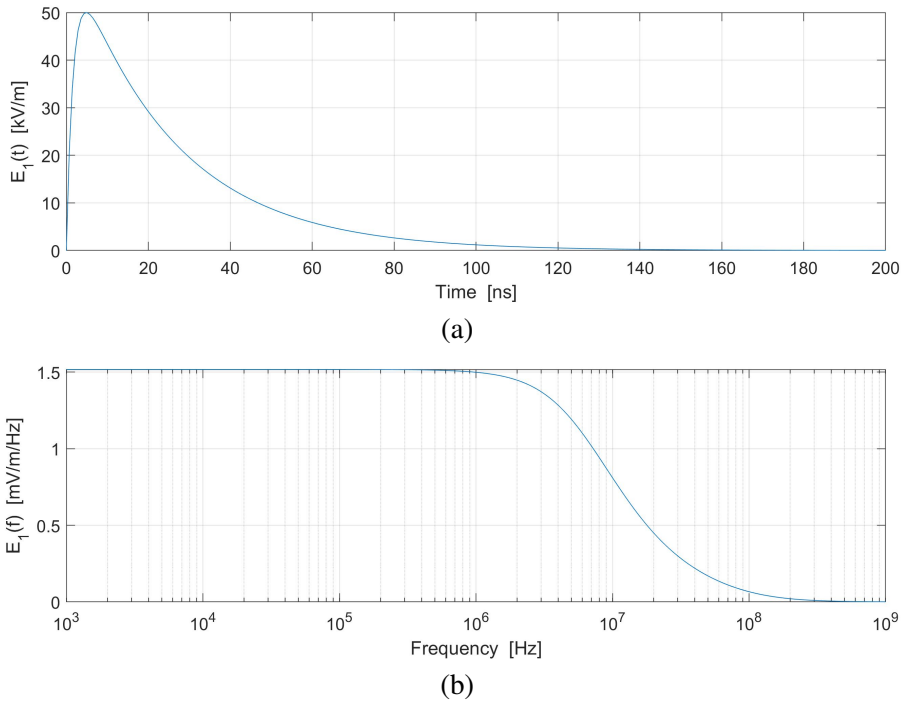

Figure 18. E1 HEMP waveform: (a) time domain; (b) frequency domain.

of the equivalent circuits mentioned previously; specifically, the phase of the transfer function takes the form

$$\angle T_E(f) = \tan^{-1}\left(\frac{f_{E,0}}{f}\right) \tag{10}$$

$$\angle T_H(f) = \tan^{-1}\left(\frac{f}{f_{H,1}}\right) - \tan^{-1}\left(\frac{f}{f_{H,0}}\right) \tag{11}$$

With the given considerations, the expected average HEMP fields inside Building 2370HVC are shown in Figure 19. Because of the high-pass filtering characteristic of the transfer functions, the waveforms coupled into the building—although reduced in their peak values—are more compressed (and have a sharper risetime) compared with the original incident signals.

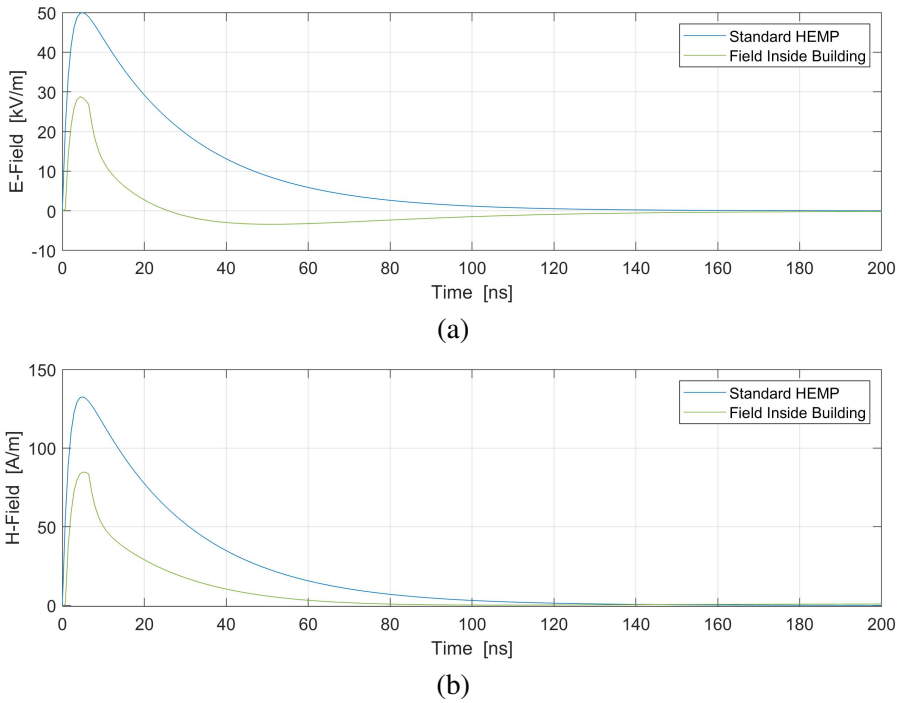

Figure 19. Interior HEMP fields for Building 2370HVC: (a) electric; (b) magnetic.

4. TESTING AT A POWER GENERATION FACILITY

Next, to further demonstrate the utility of the passive method for assessing shielding effectiveness in realistic scenarios, measurements were carried out at an actual power generation facility. The objective was to determine E1 HEMP field levels inside facility locations such as the control room, generator room, and cable spreading room. Altogether, the ambient electric and magnetic field responses were sampled inside and outside of the powerhouse building at 25 locations. Because data collection along the perimeter of the building could not be easily arranged, the exterior measurement set taken on the main roof was used as the reference for evaluating the shielding levels at interior positions. In processing the data, as done for the signals collected at the ORNL campus, transfer functions were first deduced from the measurements; subsequently, the expected E1 pulse waveforms and peak fields at various interior locations were derived.

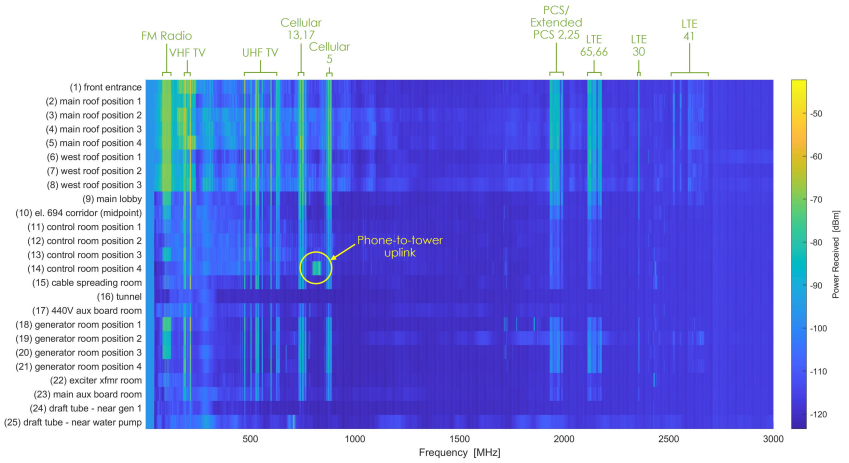

Figure 20. High-band, electric field response for the powerhouse.

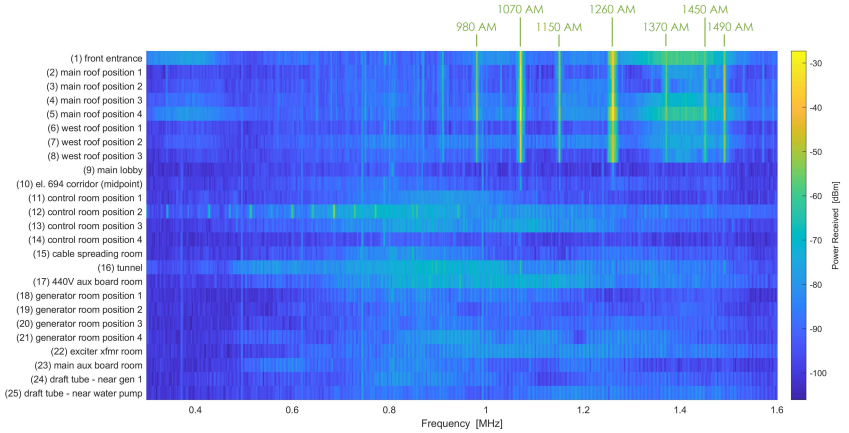

Figure 21. Low-band, electric field response for the powerhouse.

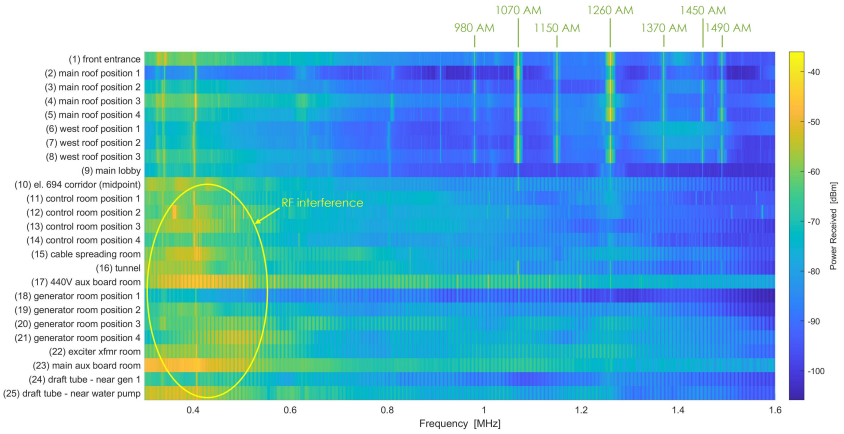

Figure 22. Low-band, magnetic field response for the powerhouse.

Table 3. Shielding effectiveness (in decibels) for the powerhouse

Location \ Frequency Band	AM Radio (~1 MHz)	FM Radio (~100 MHz)	~200 MHz	~500 MHz	~700 MHz	~900 MHz	~1900 MHz	~2100 MHz
(1) front entrance	-	-	-	-	-	-	-	-
(2) main roof position 1	-	-	-	-	-	-	-	-
(3) main roof position 2	-	-	-	-	-	-	-	-
(4) main roof position 3	-	-	-	-	-	-	-	-
(5) main roof position 4	-	-	-	-	-	-	-	-
(6) west roof position 1	-	-	-	-	-	-	-	-
(7) west roof position 2	-	-	-	-	-	-	-	-
(8) west roof position 3	-	-	-	-	-	-	-	-
(9) main lobby	45 (25)	2	4	12	4	8	9	8
(10) el. 694 corridor (midpoint)	43 (22)	5	7	21	7	16	16	16
(11) control room position 1	>59 (>34)	3	11	18	16	24	24	22
(12) control room position 2	>45 (>32)	7	11	9	17	24	25	21
(13) control room position 3	>43 (>39)	2	15	11	15	22	22	19
(14) control room position 4	>56 (29)	17	17	21	17	25	24	22
(15) cable spreading room	>55 (>33)	5	8	13	15	24	25	22
(16) tunnel	32 (17)	46	>51	>54	>48	>49	>32	>36
(17) 440V aux board room	>42 (>23)	13	17	30	29	41	32	>32
(18) generator room position 1	>51 (>42)	1	5	14	15	21	19	15
(19) generator room position 2	>58 (>38)	3	6	20	14	19	15	16
(20) generator room position 3	>58 (>29)	2	1	14	11	19	17	12
(21) generator room position 4	>57 (>38)	11	10	20	18	23	16	13
(22) exciter xfmr room	>49 (>28)	10	17	28	22	27	28	26
(23) main aux board room	>60 (>23)	15	16	25	20	27	24	22
(24) draft tube - near gen 1	>56 (>42)	36	44	51	42	48	>34	>30
(25) draft tube - near water pump	>53 (>33)	38	43	48	>42	>47	>28	>29

Electric ↑ ↑ Magnetic

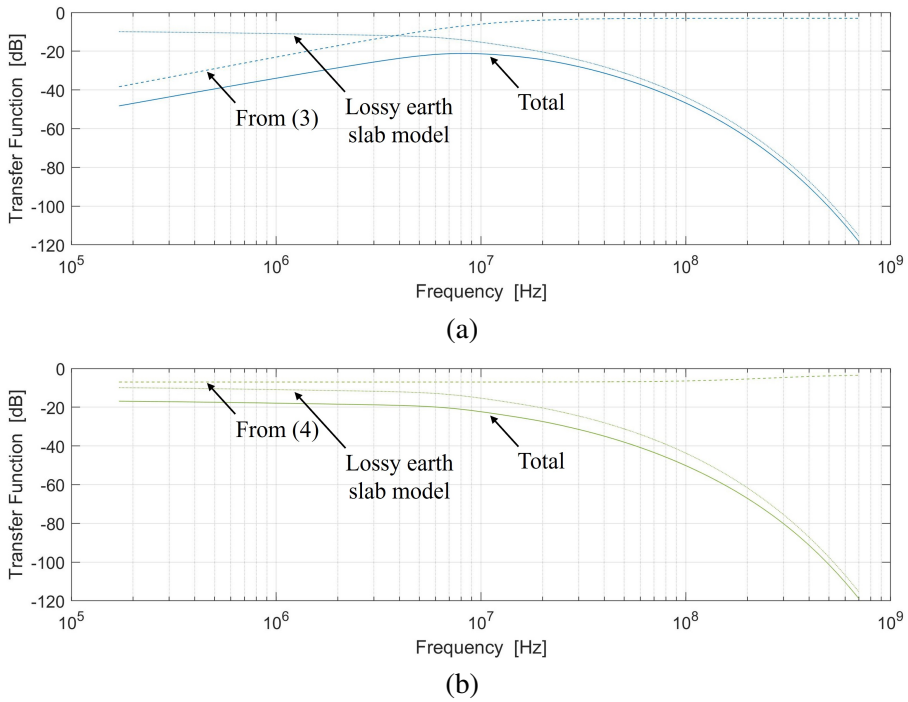

Figure 23. Transfer function models for the tunnel: (a) electric; (b) magnetic.

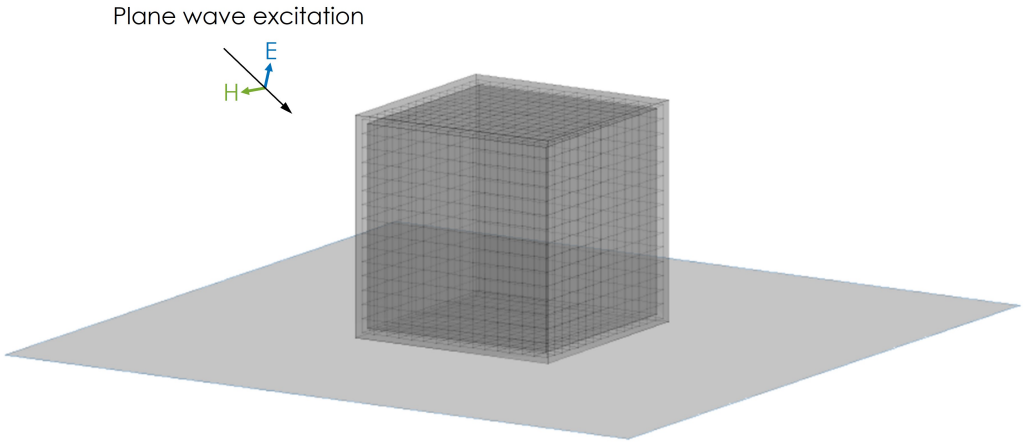

Figure 24. Canonical structure with concrete and rebars.

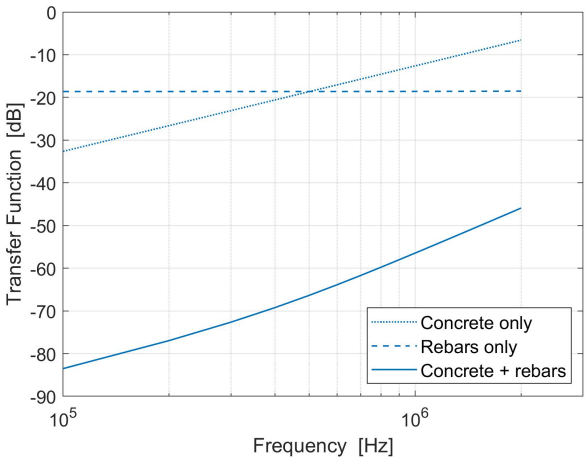

(a)

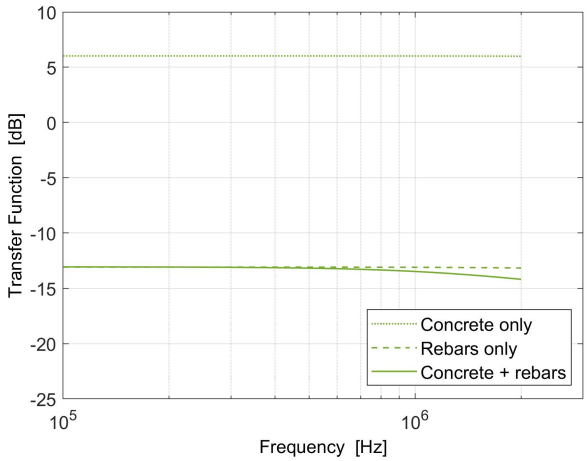

(b)

Figure 25. Simulated transfer functions for the structure in Figure 24: (a) electric; (b) magnetic.

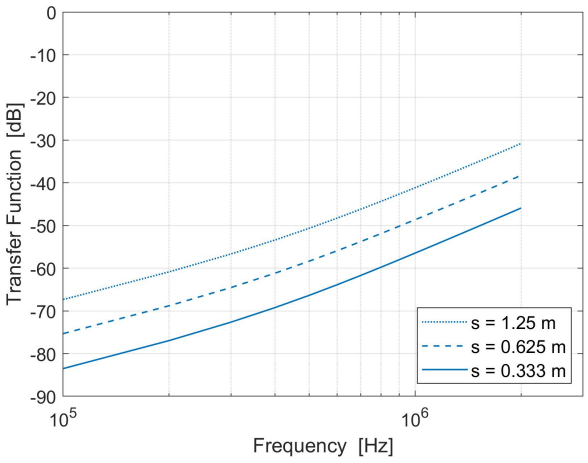

(a)

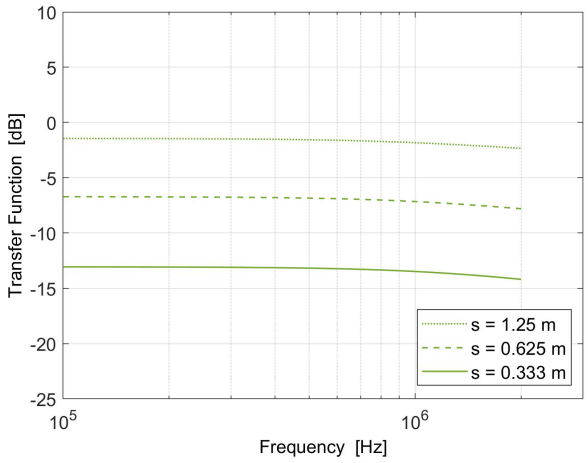

(b)

Figure 26. Simulated transfer functions for the structure in Figure 24 as a function of rebar spacing: (a) electric; (b) magnetic.

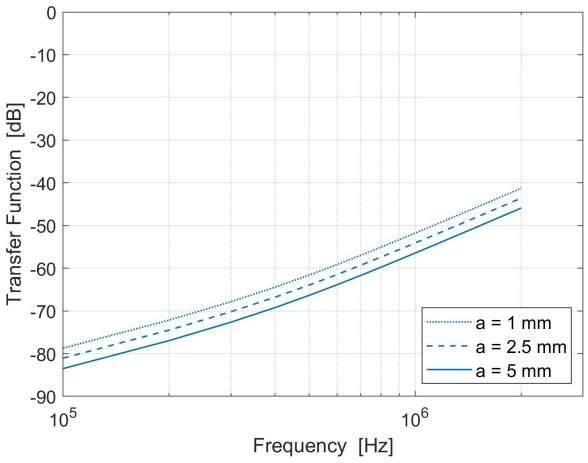

(a)

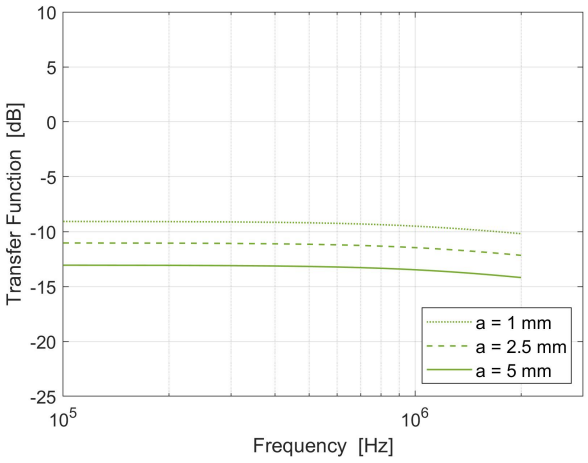

(b)

Figure 27. Simulated transfer functions for the structure in Figure 24 as a function of rebar radius: (a) electric; (b) magnetic.

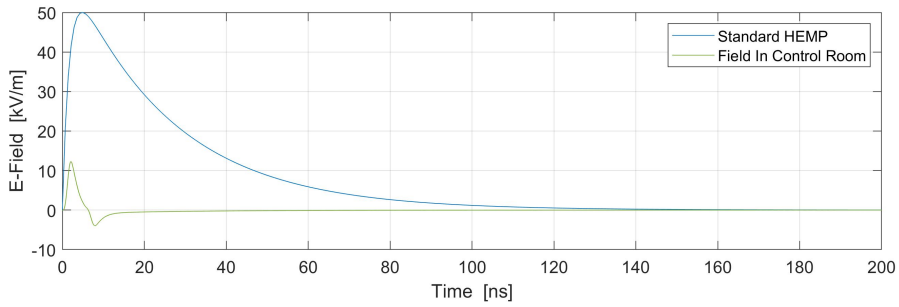

(a)

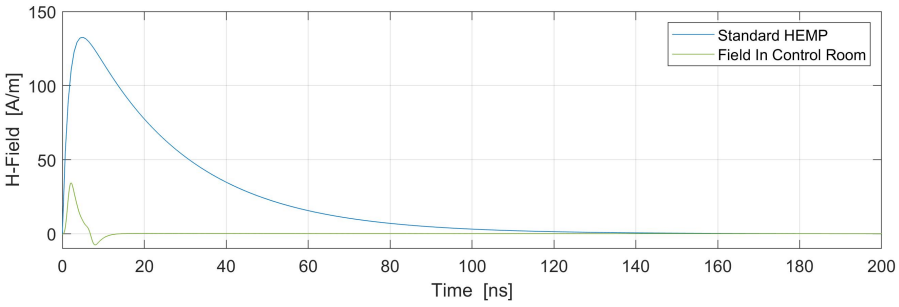

(b)

Figure 28. Interior fields for control room (average): (a) electric; (b) magnetic. Similar waveforms are found for the generator room, cable spreading room, and so on. Therefore, those results are not explicitly included here.

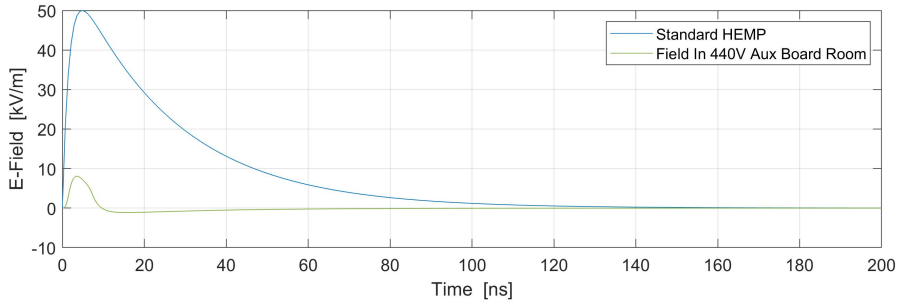

(a)

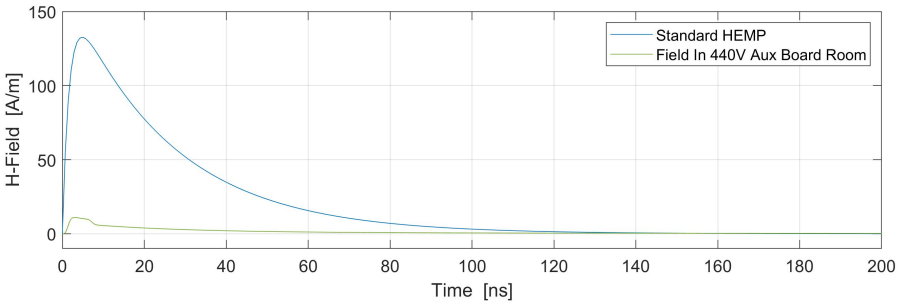

(b)

Figure 29. Interior fields for the 440 V auxiliary board room: (a) electric; (b) magnetic.

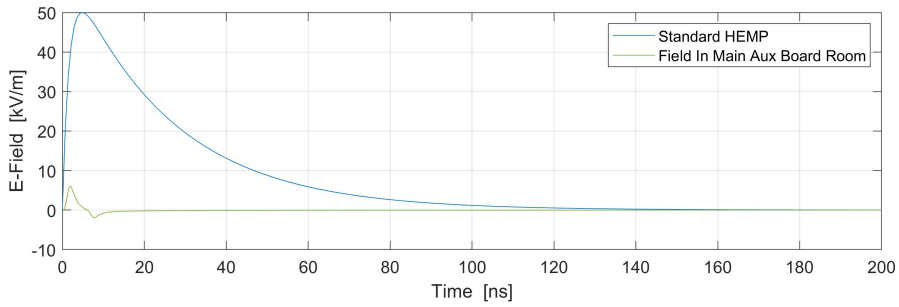

(a)

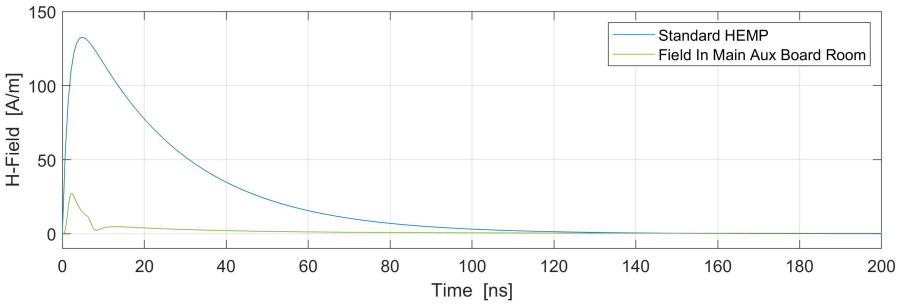

(b)

Figure 30. Interior fields for the main auxiliary board room: (a) electric; (b) magnetic.

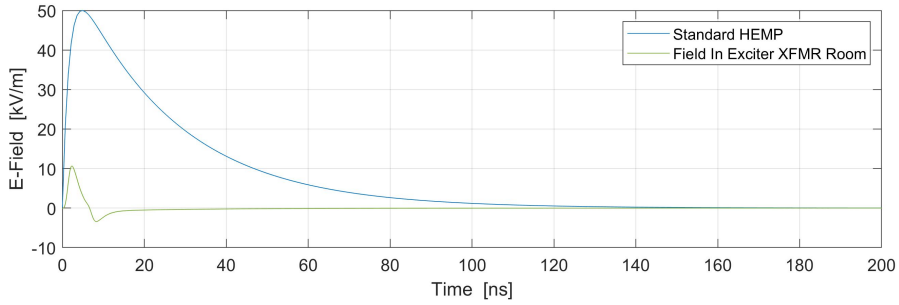

(a)

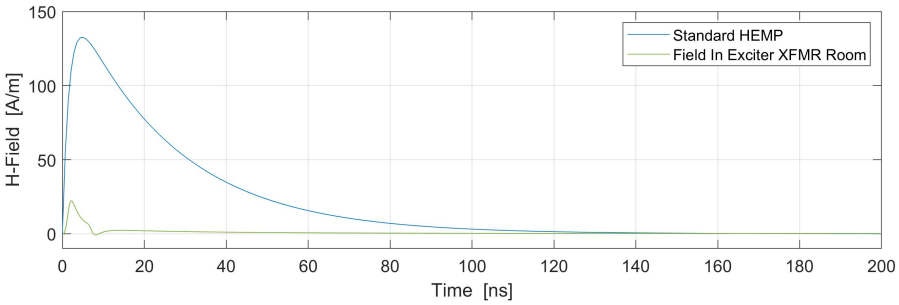

(b)

Figure 31. Interior fields for the exciter transformer room: (a) electric; (b) magnetic.

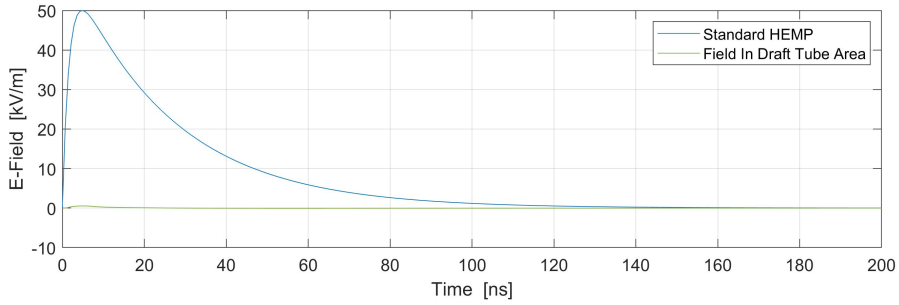

(a)

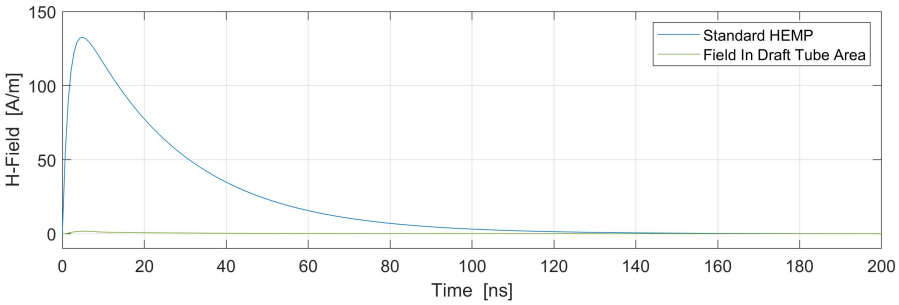

(b)

Figure 32. Interior fields for the draft tube area (average): (a) electric; (b) magnetic.

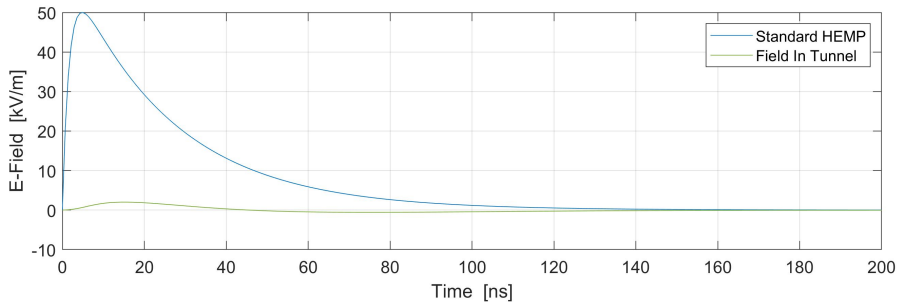

(a)

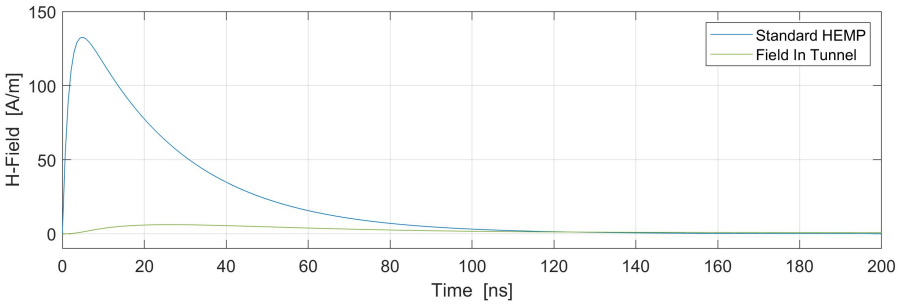

(b)

Figure 33. Interior fields for the tunnel: (a) electric; (b) magnetic.

Table 4. Parameters of coupled waveforms

Parameter of Interest / Location	Electric				Magnetic			
	t_r [ns]	t_w [ns]	E_{peak} [kV/m]	E_{peak} attenuation (time domain)	t_r [ns]	t_w [ns]	H_{peak} [A/m]	H_{peak} attenuation (time domain)
control room (average)	1.1	2.3	12.3	4.1 (12.2 dB)	1.1	2.5	34.3	3.9 (11.7 dB)
440V aux board room	1.7	5.5	8.0	6.3 (15.9 dB)	1.3	8.8	11.0	12.1 (21.6 dB)
main aux board room	1.0	2.1	6.1	8.2 (18.3 dB)	1.1	4.0	27.4	4.8 (13.7 dB)
exciter xfmr room	1.2	2.8	10.6	4.7 (13.5 dB)	1.2	3.2	22.3	5.9 (15.5 dB)
draft tube area (average)	2.3	7.7	0.5	100.0 (40.0 dB)	2.5	14.1	1.7	78.0 (37.8 dB)
tunnel	8.3	24.4	2.0	25.0 (28.0 dB)	12.7	63.8	6.1	21.7 (26.7 dB)

4.1 MEASUREMENT RESULTS

As before, at each sampling position, three sets of measurements were obtained: (1) high-band, electric field; (2) low-band, electric field; and (3) low-band, magnetic field. The assumption again was that the high-band magnetic field attenuation is approximately equal to that of the electric field. The antennas used were the same as those shown in Figure 11. For ease of interpretation, the signal spectrums from all locations were combined into a single "mosaic" plot as a function of frequency, as displayed in Figures 20–22.

Figure 20 shows the high-band, electric field response obtained with the mini-bicon antenna. The available signals over the measured frequency range included FM radio, VHF TV, ultra high frequency (UHF) TV,

and various cellular bands. In general, these signals become weaker as one proceeds deeper into the lower levels of the facility, with an increase in attenuation that becomes more evident at the higher frequencies than at the lower frequencies.

The low-band, electric field response from the monopole antenna is displayed in Figure 21. The only ambient signals present were broadcast signals from AM radio stations, most of which were situated less than ~10 mi away and to the southwest side of the test site. There was significant attenuation inside the facility at these frequencies. Among all the interior positions, the strongest signal was the one measured in the tunnel connecting the powerhouse to the switchyard. Also, considerable RF interference limited the dynamic range of the measurements.

Figure 22 displays the low-band, magnetic field data as received by the ferrite rod antenna. For the electric field response, the only signals available were those from AM radio stations. The strongest signals corresponded to those measured in the tunnel. In general, the attenuation level for interior building locations was greater than 20 dB. Once again, dynamic range was negatively affected by a significant level of interference—emitted by the internal equipment—that was mostly around the 400 kHz range but extended well into the AM radio bands.

The shielding effectiveness at the building interior and in the tunnel was calculated with Eq. (2), and the results are displayed in Table 3. At low frequencies (~1 MHz), the building structure in general provides a relatively high level of shielding, with a minimum of at least 42 dB for the electric field and 22 dB for the magnetic field. The least amount of shielding was observed in the tunnel, for which the electric and magnetic shielding levels were 32 dB and 17 dB, respectively.

At the FM radio bands, for non-tunnel locations, the attenuation appeared to be much less than that at ~1 MHz. At one location in the control room, only 2 dB of shielding was noted, and, similarly, in the generator room, the shielding fell to as low as 1 dB. The highest level of attenuation, at ~100 MHz, was experienced by signals propagating into the tunnel, for which the shielding was even higher than for locations situated deep in the facility (e.g., near the draft tube area).

At the higher frequencies (VHF TV, UHF TV, and cellular bands), the attenuation in general increased with frequency, but the shielding levels were consistently lower than those at ~1 MHz. At these frequencies, for non-tunnel locations, the dominant signal propagation mechanisms are likely defined by transmission through building apertures (e.g., windows) and diffraction around building structures, whereas for inside the tunnel, which experiences a higher level of attenuation over these bands, the propagation mode consists of transmission through the combination of a lossy soil layer and the tunnel wall.

4.2 POWERHOUSE ATTENUATION AND SIGNAL MODELS

In view of the observations described in the previous section, semi-empirical attenuation models were developed to fit the measurement data. For non-tunnel locations, which are shielded by one or more layers of reinforced concrete (i.e., a combination of concrete and rebar), the shielding functions from Eqs. (3) and (4) are satisfactory in modeling the electric and magnetic responses. The propagation behavior in the tunnel—and its attenuation profile—as evident from Table 3 is very different from at other interior locations in the facility; that is, unlike the responses at other locations, the high-frequency (~100 MHz) attenuation in the tunnel is actually greater than the low-frequency (~1 MHz) attenuation. This is partially because the tunnel is buried under a layer of ground soil, which exhibits an attenuation constant that increases exponentially with frequency at a faster rate than that for concrete. Consequently, the simple models for the

transfer functions developed previously for building interior locations become inadequate for the tunnel; however, a more complete model can be established by supplementing Eqs. (3) and (4) with an exponential term that includes the effects of a lossy soil slab. Figure 23 shows the derived total transfer functions that are appropriate for use inside the tunnel. The standard shielding models as expressed by Eqs. (3) and (4) do not provide sufficient attenuation in the high-frequency regime, whereas the lossy earth slab model by itself underestimates the attenuation in the low-frequency regime. Only by combining the two models can an attenuation profile that more accurately reflects the trends observed in the measurement data be obtained.

Notably, the measured attenuation in the low-frequency regime at the power generation facility is, in general, markedly higher than that previously recorded at Building 2370HVC. The main reason for this difference is the fact that the powerhouse is constructed of reinforced concrete, whereas the walls of Building 2370HVC are mostly composed of drywall/concrete with a metal frame—one that is likely defined by relatively widely spaced metal columns/trusses. To investigate the attenuation levels of reinforced concrete, full-wave simulations of the structure shown in Figure 24 were carried out with the method of moments. Specifically, three compositions for the outer shell of the structure were considered: (1) concrete only; (2) rebars only; and (3) rebars embedded in a layer of concrete. The low-frequency responses of the model are displayed in Figure 25. For the electric field, neither the concrete nor the rebar grid by itself would generate the high level of attenuation observed in the measurement data; the shielding effectiveness significantly increases when concrete and rebars are combined. However, for the magnetic field, most of the shielding appears to be provided by the rebars. Figures 26 and 27 show that the attenuation level, as expected, tends to increase with decreasing rebar spacing and increasing rebar radius.

4.3 INTERIOR FIELD CALCULATION AND RESULTS

With the transfer function models established, the predicted E1 HEMP signals at various locations within the powerhouse were derived using the procedure outlined in Section 3.2. The resulting waveforms are illustrated in Figures 28–33, and a summary of the waveform parameters is presented in Table 4. For non-tunnel locations, the signal transmitted into the facility was a weakened pulse with a shorter risetime and duration than the original waveform, owing to the high-pass filtering behavior of the wall material. For the tunnel, which essentially acts as a band-pass filter for the electric field but a low-pass filter for the magnetic field, the signal is not only weakened but also stretched in time, an attribute that is more evident for the magnetic field than the electric field.

5. SUMMARY

The utility of a passive approach for determining facility E1 HEMP shielding effectiveness was investigated in this study. As an initial step, electromagnetic simulations were first carried out to assess signal penetration as functions of frequency, incidence angle, building/ground plane electrical properties, and building dimensions. Although computational resource constraints limited the maximum frequency and electrical size of the problem considered, the results still informed important trends in the field response. (Structural elements such as apertures—e.g., windows and doors—and cable penetrations were omitted in the current simulation study. Of course, the coupling effects stemming from these features manifested themselves in the measurement data. Their specific levels of significance in providing additional pathways for EM wave propagation will be further considered in future investigations.)

Measurement campaigns were undertaken at the ORNL campus to identify the testing equipment needed—and to develop a systematic measurement procedure—for estimating ambient signal propagation into facility interiors. Subsequently, on-site testing was performed at a power generation plant to fully evaluate the practicality of the overall method. As a result of these efforts, a shielding effectiveness table was established for various locations within the plant, such as the control room, generator room, and cable spreading room. After the measurement-based transfer functions were fitted with appropriate attenuation models, interior HEMP waveforms were derived for the electric and magnetic fields. The following trends were observed from the power generation facility data, as relevant for HEMP frequencies of interest. For non-tunnel interior locations, in the low-frequency range (~1 MHz), the attenuation was at least 50/22 dB on average for the electric/magnetic field; in the high-frequency range (~100 MHz), except in the draft tube area and the tunnel, the average attenuation was only ~7 dB for both field components. Overall, a ~20 dB/decade attenuation rate was noted within the ~1 to ~100 MHz region, which matches a behavior previously seen in the simulations. In the tunnel, as compared with other interior locations, the attenuation at ~100 MHz was significantly higher because of soil propagation loss, whereas the attenuation at ~1 MHz was lower. The signal penetrating into the facility was, in general, a temporally compressed pulse for non-tunnel locations but a stretched one for the tunnel area. The estimated waveforms can be used as excitation sources for determining HEMP effects on various power generation equipment as part of the next phase of the study.

6. REFERENCES

[1] F. Tesche, "CW test manual," tech. rep., NEMP Laboratory, Spiez, 1994.

[2] D. Ericson, D. Strawe, S. Sandberg, V. Jones, G. Rensner, R. Shoup, R. Hanson, and C. Williams, "Interaction of electromagnetic pulse with commercial nuclear power plant systems," tech. rep., Sandia National Laboratories, 1983.

[3] "High-altitude electromagnetic pulse (HEMP) protection for ground-based C4I facilities performing critical, time-urgent missions, part 1, fixed facilities: MIL-STD-188-125-1," tech. rep., Department of Defense, Jul. 1998.

[4] P. Barnes and J. Marable, "Transient response of nuclear power plant cables to high-altitude nuclear electromagnetic pulse (EMP)," Tech. Rep. ORNL-5152, Oak Ridge National Laboratory, 1976.

[5] E. B. Savage, J. L. Gilbert, W. A. Radasky, and M. J. Madrid, "An alternative EM shielding effectiveness measurement method for buildings," in *2010 Asia-Pacific International Symposium on Electromagnetic Compatibility*, pp. 138–141, 2010.

[6] E. B. Savage, J. L. Gilbert, and W. A. Radasky, "Expedient building shielding measurement method for HEMP assessments," *IEEE Transactions on Electromagnetic Compatibility*, vol. 55, no. 3, pp. 508–517, 2013.

[7] A. A. Smith, "Attenuation of electric and magnetic fields by buildings," *IEEE Transactions on Electromagnetic Compatibility*, vol. EMC-20, no. 3, pp. 411–418, 1978.

[8] L. Rice, "Radio transmission into buildings at 35 and 150 mc," *The Bell System Technical Journal*, vol. 38, no. 1, pp. 197–210, 1959.

[9] E. Walker, "Penetration of radio signals into buildings in the cellular radio environment," *The Bell System Technical Journal*, vol. 62, no. 9, pp. 2719–2734, 1983.

[10] A. Davidson and C. Hill, "Measurement of building penetration into medium buildings at 900 and 1500 MHz," *IEEE Transactions on Vehicular Technology*, vol. 46, no. 1, pp. 161–168, 1997.

[11] H. Okamoto, K. Kitao, and S. Ichitsubo, "Outdoor-to-indoor propagation loss prediction in 800-MHz to 8-GHz band for an urban area," *IEEE Transactions on Vehicular Technology*, vol. 58, no. 3, pp. 1059–1067, 2009.

[12] N. J. LaSorte, Y. Burette, and H. H. Refai, "Experimental characterization of electromagnetic propagation of a hospital from 55–1950MHz," in *2010 Asia-Pacific International Symposium on Electromagnetic Compatibility*, pp. 826–829, 2010.

[13] M. Bäckström, B. Nordström, and K. G. Lövstrand, "Is HPM a threat against the civil society?," in *Proceedings of the 27th General Assembly of the URSI*, 2002.

[14] W. A. Radasky, C. E. Baum, and M. W. Wik, "Introduction to the special issue on high-power electromagnetics (HPEM) and intentional electromagnetic interference (IEMI)," *IEEE Transactions on electromagnetic compatibility*, vol. 46, no. 3, pp. 314–321, 2004.

[15] A. Bürgi, D. Scanferla, and H. Lehmann, "Time averaged transmitter power and exposure to electromagnetic fields from mobile phone base stations," *International Journal of Environmental Research and Public Health*, vol. 11, no. 8, pp. 8025–8037, 2014.

[16] R. Mittra, *Computational Electromagnetics: Recent Advances and Engineering Applications*. Springer, 2014.

[17] Feko, 2021. https://www.altair.com/feko/.

[18] "IEC 1000-2-9: Description of HEMP environment-radiated disturbance," tech. rep., IEC, 1996.

[19] "Physical characteristics of HEMP waveform benchmarks for use in assessing susceptibilities of the power grid, electrical infrastructures, and other critical infrastructure to HEMP insults." Department of Energy, Washington, DC, USA, 2021 [Online].

[20] J. Kong, *Electromagnetic Wave Theory*. Cambridge, MA: EMW Publishing, 2000.